Available online at www.sciencedirect.com
ScienceDirect
Polymer 48 (2007) 1379–1387
polymer
www.elsevier.com/locate/polymer

Experimental studies and molecular modelling of the stress–optical and stress–strain behaviour of poly(ethylene terephthalate). Part III: Measurement and quantitative modelling of birefringence–strain, stress–strain and stress–optical properties

J.I. Cail [a], L.S. Saunders [b], R.F.T. Stepto [a,*], I.M. Ward [b,**]

[a] *Polymer Science and Technology Group, School of Materials, The University of Manchester, Grosvenor Street, Manchester M1 7HS, UK*
[b] *IRC in Polymer Science and Technology, School of Physics and Astronomy, University of Leeds, Leeds LS2 9JT, UK*

Received 9 September 2006; received in revised form 18 December 2006; accepted 31 December 2006
Available online 26 January 2007

Abstract

Experimental measurements and Monte-Carlo (MC) modelling of the birefringence–strain, stress–strain and stress–optical behaviour of poly(ethylene terephthalate) (PET) are used, together with the analysis of orientation–strain and conformation–strain behaviour reported in Paper I, to give a detailed, quantitative interpretation and characterisation of its deformation-related properties. The difference between the stress–strain and stress–optical behaviour of PET that had been reported previously is confirmed. Except for the stress, the measured values of all the properties studied are in agreement with those calculated using the MC modelling, which suggests that not all of the junctions or the chains in the entangled PET network are elastically active.

The results given by Kuhn and Grün theory are compared with those given by the MC modelling. The expected shortcomings of Kuhn and Grün theory are found. However, distinct from the behaviour reported previously for polyethene, the theory can be used to evaluate, semi-empirically, the stress–optical coefficient of PET.

Keywords: Poly(ethylene terephthalate); Birefringence; Monte-Carlo modelling

1. Introduction

The birefringence of a polymer has been long recognised as a valuable tool for estimating the molecular orientation that can arise during melt extrusion or the subsequent stretching processes during or after solidification. The classical interpretation of the stress–birefringence and strain–birefringence behaviour of a rubber is provided by the Kuhn and Grün theory [1,2], based on Gaussian, freely-jointed chains. However, recent studies by Stepto and coworkers [3–6], modelling Saunders' data [7] for polyethene (PE), have shown that the Kuhn and Grün theory is not quantitatively accurate for that polymer. In contrast, using the Monte-Carlo (MC) network model of Stepto and Taylor [8,9], combined with detailed calculations of segmental orientations, it was possible to calculate exactly [3,4,6] the experimental values [7] of the stress–optical coefficient, C, of PE and the dependence of C on the molar mass of the network chains. Key to the quantitative modelling of experimental data is (1) an accurate rotational-isomeric-state (RIS) model of the polymer chain being studied; (2) a network model that does not treat all chains as the "average" network chain, but accounts for the different stresses developed by chains lying at different angles to the strain direction, as well as for the non-affine behaviour of individual chains; (3) a detailed evaluation of average segmental orientations in external co-ordinates as functions of strain; and (4) correct values of bond polarisabilities.

* Corresponding author. Tel./fax: +44 1625 872581.
** Corresponding author. Tel.: +44 113 343 3808; fax: +44 113 343 3846.
E-mail addresses: rfts@tesco.net (R.F.T. Stepto), i.m.ward@leeds.ac.uk (I.M. Ward).

0032-3861/$ - see front matter © 2007 Elsevier Ltd. All rights reserved.
doi:10.1016/j.polymer.2006.12.050

In this paper, we address the more difficult problem of the stress–optical behaviour of poly(ethylene terephthalate), for which there are two distinctly different methods of producing molecular orientation. Firstly, significant orientation can be produced by winding-up tapes or filaments at moderate or high wind-up speeds. Secondly, extruded sheets or filaments can be stretched, most usually at temperatures just above the glass-transition temperature, T_g, where homogeneous deformation can be obtained. It has been shown that, in both cases, a satisfactory approach to obtain quantitative predictions of the molecular orientations is to assume that they are developed in a manner similar to that expected for a rubber-like network [10–12]. In the case of the fibre-spinning process, it can be considered that the filaments cool rapidly to form an entangled network which is stretched due to the tension in the threadline. For comparatively low degrees of orientation, where crystallisation has not occurred, the oriented filament is akin to a frozen stretched rubber and, if subsequently heated above T_g, a ''shrinkage stress'' is developed which has been interpreted as a rubber-like entropic stress. In the case where an extruded non-crystalline sheet or filament is stretched at temperatures just above T_g, a similar interpretation has often been made, *i.e.*, it is assumed that, for draw ratios below about 2.5, where no crystallisation is observed, the orientation process is again akin to the stretching of a rubber-like network [13].

The Kuhn and Grün model has therefore been applied extensively to the deformation behaviour of PET, and it has been very successful in producing consistent correlations between stress, strain and birefringence for spun yarns, drawn fibres and drawn films [13]. A key result of the Kuhn and Grün model is that there is a direct proportionality between the stress and the birefringence, *i.e.*, a constant stress–optical coefficient. Because it is more difficult to measure the stress than the birefringence in the spin line, this simple relationship has proved very useful to fibre technologists.

The Kuhn and Grün model is, however, not based on an understanding of the actual molecular structure. In view of the development by Stepto and coworkers of the detailed MC molecular modelling of stress–optical behaviour [3–6], it has therefore been appropriate to revisit this area of research on PET and provide experimental support by infra-red measurements of changes in molecular conformation and molecular orientation, in addition to measurements of birefringence and shrinkage force. Previous investigations [10–12,14,15] have been directed at the stress–optical behaviour of spun fibres or the measurement of molecular orientation by spectroscopic methods (infra-red, Raman, or NMR). None of the previous studies has involved a comprehensive set of measurements, such as those described in the present group of papers, and the interpretation has always been based either on the Kuhn and Grün model or on the Ward aggregate model [16], both of which are based on simple phenomenological modelling rather than actual molecular behaviour.

Unfortunately, initial application of the MC approach to modelling the stress–optical behaviour of PET did not meet with the same success [17] as that achieved for PE. Apparently, higher values of birefringence were measured than would have been predicted from the observed stress–strain behaviour (modulus) of the networks. The investigation and unravelling of the origins of this inconsistency have been complicated, resulting in the present group of three papers. They have necessitated, as described in Paper I [18], direct measurements of conformer populations and segment orientations as functions of strain, as well as their detailed modelling using individual bond orientations and conformations. These measurements and calculations have confirmed the particular RIS model appropriate for bulk PET [19–21] and the applicability of the MC-modelling method to that polymer. Following the work in Paper I, Paper II [22] has described the computational protocols for calculating birefringence ($\Delta\tilde{n}$) taking account of the detailed geometry of the PET chain and the conformational dependence of the polarisabilities of the glycol segments.

The present paper uses new experimental birefringence–strain and stress–strain measurements on PET together with the RIS model from Paper I and the computational protocols of Paper II for calculating values of $\Delta\tilde{n}$ to give a quantitative modelling of the measured birefringence–strain properties of PET. In addition, the reason for the difference between stress–strain and stress–optical (birefringence–stress) properties noted previously [17] is resolved.

2. Experimental studies

With PET it is possible to produce oriented material having a moderate but significant degree of molecular orientation but no crystallinity. As stated, this can be achieved, either by melt-spinning and winding-up tapes or filaments at moderate wind-up speeds, or by tensile drawing above the glass-transition temperature, T_g, to modest draw ratios and, in both cases, rapid quenching to room temperature. The oriented material is akin to a frozen, stretched elastomer, so that, if it is subsequently heated to a temperature above T_g, an entropic stress is developed [10–13].

In the present work, the sample of PET used in Paper I, of $M_n \approx 1.95 \times 10^4$ g mol^{-1} (chains of *ca.* 100 repeat units), was used. It had been melt extruded at 533–553 K and quenched to room temperature [23]. As described in Paper I, tensile-test-piece samples were made, drawn uniaxially at 85 °C to various deformation ratios, λ, and quenched again to room temperature. Infra-red (IR) measurements were used to determine, as functions of λ, the percentage of *gauche* glycol conformers and the average orientation of terephthaloyl units to the draw direction. The densities, ρ, were also measured. In addition, for the present paper, $\Delta\tilde{n}$ was measured and, finally, the true shrinkage stresses, t, were measured after heating the samples to 80 °C and allowing the entropic shrinkage force to develop. The values of the various quantities determined experimentally will be shown in figures in this paper, alongside their predicted values.

3. Monte-Carlo modelling

The Monte-Carlo (MC) modelling of segmental orientation and birefringence in Papers I and II, respectively, is

extended in the present paper to include stress–strain behaviour. Details of the MC network stress–strain modelling method, particularly as applied to PET, have been given elsewhere [20,21].

The temperature for the calculations was set at 523 K, as for the calculations of Papers I and II and the previous modelling [19] of the experimental values of $(\langle r^2\rangle/M)_\infty$. As stated in Paper I, it was checked that the use of 523 K rather than a temperature within the temperature range at which the PET sample was formed, 533–553 K, produced negligible changes in the properties calculated.

4. Comparison of experimental and MC modelling results

4.1. Orientation–deformation and conformation–deformation behaviours

In Paper I, it was shown that the new MC RIS model for PET [19–21] predicted the changes in the average orientation of the terephthaloyl segments and in the *gauche* glycol conformations on drawing. The experimental data, based on IR measurements, could be fitted well on the basis of a network of PET chains of about 10 repeat units in length. These experimental and modelling results were summarised in Figs. 7 and 9 of Paper I.

4.2. Birefringence–deformation behaviour

Paper II described the protocols for calculating the birefringence of drawn samples and these have been used to produce the curves in Fig. 1(a) and (b) of the present paper. Fig. 1(a) shows the birefringence–deformation behaviour of PET up to a deformation ratio, λ, of $\lambda \approx 2$ and Fig. 1(b) up to $\lambda \approx 5$. In both figures, birefringence, $\Delta\tilde{n}$, is plotted *versus* $\lambda^2 - \lambda^{-1}$. The calculated curves for chain lengths of 8–12 repeat units, using the bond polarisabilities of Denbigh [24], are equivalent to those of Fig. 10 of Paper II. (Indeed, the same calculated results for the chain length of 10 repeat units are shown in Fig. 1(a) and (b) of the present paper and in Fig. 10 of Paper II.)

There is scatter apparent in the experimental values of $\Delta\tilde{n}$ in Fig. 1(a). (There are negligible errors in the measured values of λ as they can only arise from changes in the positions of reference lines marked on the specimens.) The experimental results are situated around the calculated values of $\Delta\tilde{n}$ for chains of between 9 and 10 repeat units. Use of the Bunn and Daubeny [25] or the LeGrand and Scacchetti bond polarisabilities [26] gives calculated curves of the same shape but shifted with respect to those in Fig. 1(a). The Bunn and Daubeny bond polarisabilities result in the experimental results being situated around the calculated values of $\Delta\tilde{n}$ for a chain of 9 repeat units and the LeGrand and Scacchetti bond polarisabilities mean the experimental results are situated around the calculated values of $\Delta\tilde{n}$ for a chain of 11 repeat units. All these behaviours can be considered consistent with the variations in terephthaloyl orientation and glycol conformation with deformation analysed in Paper I, according to which entangled PET networks behaved as networks of chains of about 10 repeat units in length.

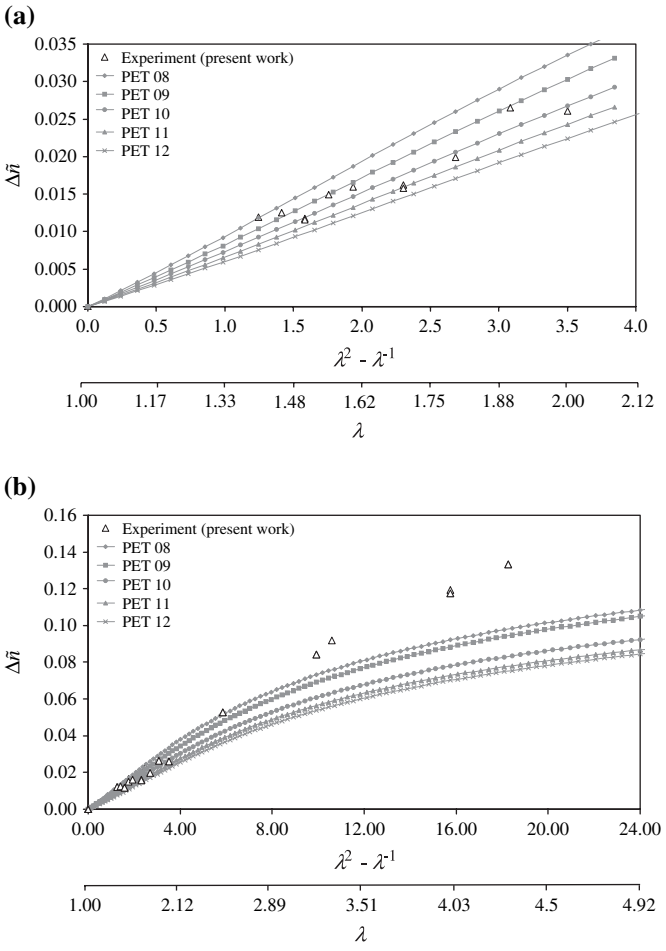

Fig. 1. Experimental and calculated birefringence–deformation behaviour of PET plotted as $\Delta\tilde{n}$ *versus* $\lambda^2 - \lambda^{-1}$, with λ the deformation ratio. (a) Results up to $\lambda \approx 2$. (b) Results up to $\lambda \approx 5$. The calculated values of $\Delta\tilde{n}$ are for chains of 8–12 repeat units at 523 K according to Denbigh bond polarisabilities [24].

The general agreement between experiment and calculation at the lower values of λ is perhaps more clearly seen in Fig. 1(b). Also, in that figure, the effects of crystallisation are apparent above $\lambda \approx 2.5$ when $\Delta\tilde{n}$ becomes increasingly larger than expected as crystallisation increases. This behaviour is in agreement with that discussed in Paper I in relation to the change of % *gauche* glycol conformations with deformation. Fig. 7 of Paper I shows that a faster decrease in % *gauche* glycol conformations than expected occurs for $\lambda > 2.5$, consistent with the onset of crystallisation and indicating an enhanced transformation of the glycol units from *gauche* to *trans*, the latter being the only conformation present in crystalline regions.

4.3. Stress–strain behaviour

Fig. 2 shows the measured and predicted stress–strain behaviour, with reduced true stress, $t/RT\rho$, plotted *versus*

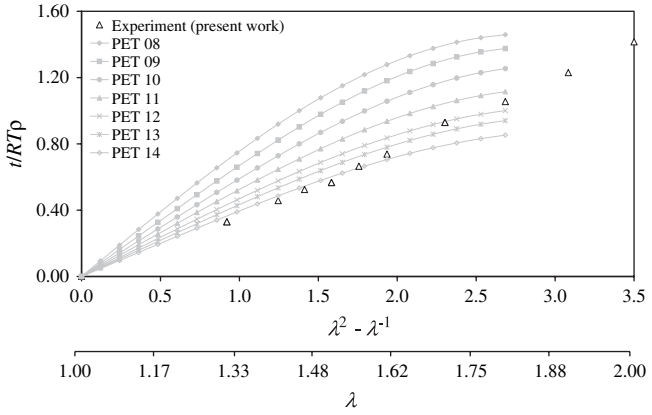

Fig. 2. Experimental and calculated stress–strain behaviour of PET plotted as reduced true stress, $t/RT\rho$, *versus* $\lambda^2 - \lambda^{-1}$. Calculated curves from MC modelling of networks of chains of 8–14 repeat units in length at 523 K.

$\lambda^2 - \lambda^{-1}$. t is the true stress and ρ the density. Given the successful modelling of the changes with $\lambda^2 - \lambda^{-1}$ of average orientation of the terephthaloyl segments (Paper I), % *gauche* glycol conformations (Paper I) and $\Delta\tilde{n}$ (Fig. 1) on the basis of chains of 9–11 repeat units in length, Fig. 2 shows that, particularly at the smaller deformations, lower stresses than expected have been measured. The measured stresses apparently indicate a lower modulus with an average entanglement chain length of about 15 repeat units. This larger value of the average chain length agrees with that deduced by Matthews et al. [27] from measurements on PET under pure shear. However, the present integrated studies show that a more likely explanation is that the lower modulus is due to not all of the entanglements defining the PET network of chains of 10–11 repeat units in length being able to support stress. One can envisage slip-links, as proposed by Ball et al. [28]. Alternatively, one may consider that not all of the network chains may be elastically active. Also, it may be noted that the parent chains are too long (about 100 repeat units) for the reduction in modulus to be due to inelastic loose ends. Each parent chain constitutes about 10 network chains of 10 repeat units in length. Hence, loose ends, equivalent to about one network chain per parent chain, can only account for about 10% of the network chains and a 10% reduction in modulus.

The proposed explanation of the lower modulus can be deduced from the following reasoning. The plots in Fig. 2 can be described by the equation [8,9,20]

$$\frac{t}{RT\rho} = \frac{1}{M_c}\left[2s\left(\lambda^2 - 1/\lambda\right) + \left(\lambda^3 + 2 - 3\lambda\right)\frac{ds}{d\lambda}\right], \tag{1}$$

obtained by differentiating the equation for the Helmholtz energy,

$$\Delta A/NRT = s\left(\lambda^2 + 2/\lambda - 3\right), \tag{2}$$

with respect to sample length. M_c in Eq. (1) is the molar mass of the elastically active chains and N in Eq. (2) is the number of moles of elastically active chains in the network. For a network of Gaussian chains behaving affinely, $s = 1/2$. In reality, s varies with λ in a way that is characteristic of chain structure and conformational behaviour. Accordingly, the curvature of the calculated plots in Fig. 2 is due to the variation of s with λ. The initial slopes of the plots are determined principally by the first term in Eq. (1) and are approximately equal to $2s/M_c$. However, because $N = \rho V/M_c$, where V is the volume of the network, the factor $1/M_c$ in Eq. (1) can be replaced by $(N/V)(1/\rho)$ and, as $s \approx 1/2$ for λ near 1, the initial slopes of the plots in Fig. 2 are equal to $(N/V)(1/\rho)$. Hence, the initial slopes of the plots in Fig. 2 can, in fact, be interpreted as being proportional to N/V, the molar concentration of elastically active chains, on average 9–11 repeat units in length, in the network. Accordingly, the slope of the line defined by the experimental points in Fig. 2 is from about 0.53 to 0.67 of the initial slopes of the theoretical curves for chains of 9–11 repeat units, with an average value of 0.59. Hence, only about 0.6 of the entanglements or chains defining the PET network is able to support stress. In contrast, all the entanglements or chains contribute towards restricted conformational freedom and, hence, to help define the segment-based properties, terephthaloyl orientation, % *gauche* glycol conformations and $\Delta\tilde{n}$ as functions of deformation.

4.4. Birefringence–stress (stress–optical) behaviour

Fig. 3 shows $\Delta\tilde{n}$ *versus* the reduced true stress, $t/RT\rho$, using the data from Figs. 1(b) and 2 and from earlier work [10,17]. According to Kuhn and Grün theory [1,2], both t and $\Delta\tilde{n}$ are proportional to $\lambda^2 - \lambda^{-1}$ and, hence, to each other. Their ratio, strictly as $\lambda \to 1$, defines the stress–optical coefficient, C, namely,

$$C = \left(\frac{\Delta\tilde{n}}{t}\right)_{\lambda \to 1}. \tag{3}$$

C is also predicted to be independent of molar mass.

The experimental results in Fig. 3 are all generally in agreement with one another. The theoretical curves from the detailed molecular modelling show upward curvature and only a slight sensitivity to chain length. The upward curvature

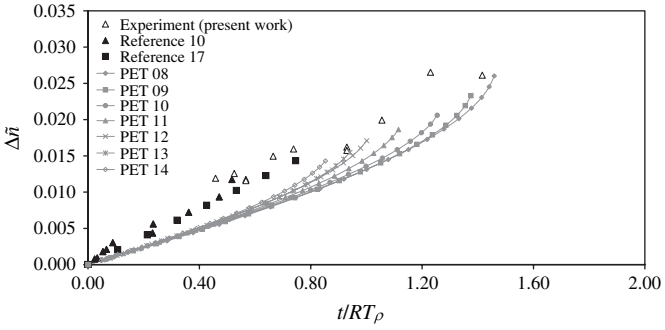

Fig. 3. Experimental and calculated birefringence–stress (stress–optical) behaviour of PET plotted as $\Delta\tilde{n}$ *versus* reduced true stress, $t/RT\rho$. Present experimental results and results from Refs. [10] and [17]. (a) Calculated curves from MC modelling of networks of chains of 8–14 repeat units in length at 523 K using Denbigh bond polarisabilities [24].

results from the nonlinear birefringence–deformation and stress–strain curves in Figs. 1(b) and 2. As discussed previously with regard to stress–strain behaviour [8,9,20], the curvature at the higher values of λ or $t/RT\rho$ may be exaggerated by the modelling. However, even at the lower values of λ or $t/RT\rho$ there is a significant difference between experiment and theory apparent in Fig. 3. This was the discrepancy that had been noted previously [17] and was then attributed to the distribution of entangled chain lengths, with the shorter chains becoming more highly extended and leading to larger values of $\Delta\tilde{n}$ being measured than were expected. In contrast, the present work, with its combined measurements and modelling of several properties (terephthaloyl orientation, % *gauche* glycol conformations, $\Delta\tilde{n}$ and t) of the same samples as functions of $\lambda^2 - \lambda^{-1}$ suggests that it is in fact the measured stress that is the inconsistent property.

In Fig. 3, the experimental results at the lower values of $\Delta\tilde{n}$ define a slope ($=C/RT\rho$) that is about 1.5 times the expected value on the basis of the Denbigh bond polarisabilities. Thus, if the experimental values of t are increased by a factor 1.5, agreement with the MC-modelling results is obtained. Use of the lower Bunn and Daubeny bond polarisabilities gives similar calculated curves, but with lower slopes. They would require the experimental values of t to be increased by a factor of about 1.7 to give agreement with the modelling results. On the other hand, use of the higher LeGrand and Scacchetti bond polarisabilities would require the experimental values of t to be increased by a factor of about 1.3 to give agreement with calculation.

4.5. Summary

Overall, the terephthaloyl orientation and glycol conformation (Section 4.1) and birefringence (Section 4.2) of PET are correctly modelled as functions of deformation using network chains of 9–11 repeat units in length and the RIS chain model appropriate for bulk PET. Stress is the one property on which experiment and modelling do not agree. Lower values of stress are measured than those predicted by modelling. The simplest explanation of this phenomenon is that not all of the chain entanglements defining the PET network are of sufficient stability to be able to support stress or not all of the PET chains are elastically active. This explanation is in contrast with that published earlier [17] on the basis of less comprehensive measurements, when it was assumed that the stress had been measured correctly and, hence, it was deduced that larger values of birefringence than expected had been measured.

5. Comparison of MC-modelling results for PET and polyethene (PE) with classical Kuhn and Grün behaviour

It is important to compare the relationships between orientation and stress and strain that are predicted by the detailed MC modelling of PET and PE [3–6] with those given by the classical treatment of Kuhn and Grün [1,2], based on Gaussian, freely-jointed chains. From the comparison, the shortcomings and usefulness of the Kuhn and Grün approach can be assessed.

Fig. 4 shows $\langle P_2(\cos\zeta_{rep})\rangle$ *versus* $\lambda^2 - \lambda^{-1}$ for PET chains of 8, 11 and 14 repeat units. As expected, orientation increases as chain length decreases. Close inspection of the MC-modelling results shows that they give curves with slopes that first increase and then decrease as one moves away from the origin in both the positive and negative directions. In contrast, Gaussian Kuhn and Grün theory predicts straight lines that follow the equation

$$\left\langle P_2\left(\cos\zeta_{rep}\right)\right\rangle = \frac{1}{5m}\left(\lambda^2 - \lambda^{-1}\right), \tag{4}$$

where m is the number of links in the freely-jointed chain equivalent to the real chain. The equivalent chain, with m links of length l', has the same mean-square and maximum end-to-end distances, $\langle r^2\rangle$ and r_{max}, as the real chain of n skeletal bonds, with

$$\left\langle r^2\right\rangle = ml'^2 \tag{5}$$

and

$$r_{max} = ml', \tag{6}$$

so that

$$m = r_{max}^2/\left\langle r^2\right\rangle. \tag{7}$$

The dashed lines in Fig. 4 are for $m = 7.49$, 10.12, 12.79, which, according to the RIS model for bulk PET [19–21], are the equivalent chains for real PET chains at 523 K of 8, 11, 14 repeat units or 48, 66, 84 skeletal bonds. (By coincidence, the number of freely-jointed links is approximately equal to the number of repeat units.) The slopes of the Gaussian Kuhn and Grün lines are significantly less than the average slopes of the curves from the detailed modelling and the

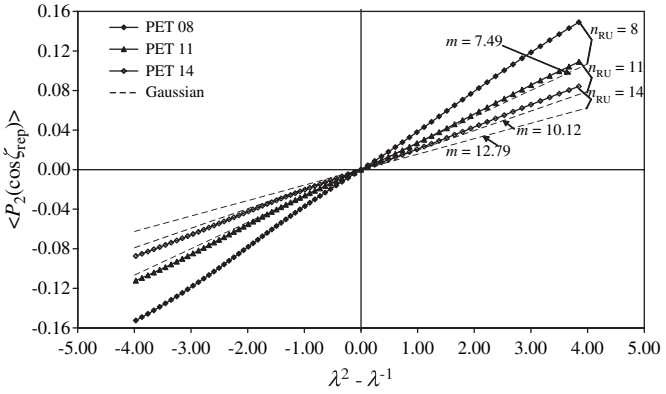

Fig. 4. Calculated PET repeat-unit orientation for PET chains at 523 K as a function of deformation, plotted as $\langle P_2(\cos\zeta_{rep})\rangle$ *versus* $\lambda^2 - \lambda^{-1}$. MC modelling of networks of chains of 8, 11 and 14 repeat units in length ($n_{RU} = 8$, 11, 14). – – –: values calculated from Kuhn and Grün theory using Gaussian chains of m equivalent freely-jointed links, with the values of m corresponding to the actual chains.

difference between the slopes decreases as chain length increases.

The corresponding MC-modelling plots of $\langle P_2(\cos\zeta)\rangle$ *versus* $\lambda^2-\lambda^{-1}$ for PE chains [4] also showed nonlinear behaviour. (For PE, ζ is the angle between a skeletal C–C bond vector and the draw direction.) However, at shorter chain lengths (*e.g.* $n=40$, where n is the number of skeletal C–C bonds) the slopes of the Gaussian Kuhn and Grün lines are lower than the average slopes of the curves from the detailed modelling, as for PET, whereas, at longer chain lengths (*e.g.* $n=80$, 220) the slopes of the Kuhn and Grün lines become higher than the average slopes of the curves from the detailed modelling. Thus, Kuhn and Grün predictions are difficult to apply as the sense and the size of their deviations from actual molecular behaviour are dependent on chain structure.

A detailed analysis of the MC-modelling results and the results of Kuhn and Grün theory for PE [4] showed that the linear relationship between $\langle P_2(\cos\zeta)\rangle$ and $\lambda^2-\lambda^{-1}$ predicted by Kuhn and Grün theory arises from the assumed independence of ξ, the angle between the segment (bond) vector and the chain end-to-end vector, and ψ, the angle between the chain end-to-end vector and the draw direction. The independence means that $\langle P_2(\cos\zeta)\rangle$ is effectively evaluated using the equation

$$\langle P_2(\cos\zeta)\rangle = \big\langle \langle P_2(\cos\xi)\rangle_i \big\rangle \cdot \langle P_2(\cos\psi_i)\rangle \tag{8}$$

based on the Legendre addition theorem [29]. $\langle P_2(\cos\xi)\rangle_i$ is the average value of $P_2(\cos\xi)$ for the segments of chain i, $\langle\langle P_2(\cos\xi)\rangle_i\rangle$ is the average value of $\langle P_2(\cos\xi)\rangle_i$ over all the chains, i, of the network, and $\langle P_2(\cos\psi_i)\rangle$ is the average value of $P_2(\cos\psi_i)$ over all the chains, i, of the network. On the other hand, the detailed MC modelling accounts for the dependence of the average segment orientation in a chain on the orientation of the end-to-end vector (*i.e.*, more extended chains tend to be more aligned to the draw direction) and $\langle P_2(\cos\zeta)\rangle$ is evaluated using

$$\langle P_2(\cos\zeta)\rangle = \big\langle \langle P_2(\cos\xi)\rangle_i \cdot P_2(\cos\psi_i) \big\rangle, \tag{9}$$

so that $\langle P_2(\cos\xi)\rangle_i$ and $P_2(\cos\psi_i)$ are not pre-averaged. (*cf.* Eq. (12) of Paper I and Eqs. (33), (46) and (51) of Paper II.) It is the interdependence of ξ and ψ that gives the nonlinear relationship between $\langle P_2(\cos\zeta)\rangle$ and $\lambda^2-\lambda^{-1}$. For PET, the same arguments hold true with ζ being ζ_{rep} and ξ being ξ_{rep}.

Following the work on PE [4], the nonlinearity of plots of $\langle P_2(\cos\zeta_{\text{rep}})\rangle$ *versus* $\lambda^2-\lambda^{-1}$ is analysed in terms of the deformation–orientation coefficient, Z_λ, defined [3,4] by the equation

$$\big\langle P_2\big(\cos\zeta_{\text{rep}}\big)\big\rangle = Z_\lambda\big(\lambda^2-\lambda^{-1}\big). \tag{10}$$

Fig. 5 shows the variation of Z_λ from the detailed MC modelling with $\Delta\lambda$ for chains of 7, 10 and 14 repeat units. (The change of the chain lengths shown between Figs. 4 and 5 is not significant.) Z_λ has been evaluated assuming $\langle P_2(\cos\zeta_{\text{rep}})\rangle$ and $\lambda^2-\lambda^{-1}$ are directly proportional to each other between $\lambda=1$ and $1+\Delta\lambda$. It should be emphasised that, relative to

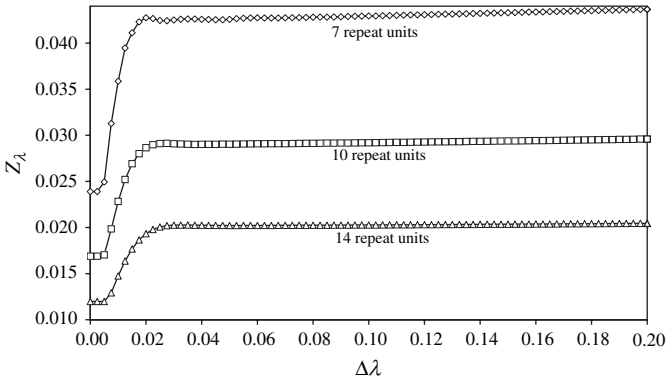

Fig. 5. Calculated deformation–orientation coefficient, Z_λ, *versus* $\Delta\lambda$, the range of deformation ratio from $\lambda=1$ over which Z_λ and $\lambda^2-\lambda^{-1}$ are assumed to be directly proportional to each other. PET chains of 7, 10 and 14 repeat units.

the range of deformations covered in Fig. 4, Fig. 5 refers to small deformations. For example, $\Delta\lambda=0.2$, or $\lambda=1.2$, the maximum deformation shown in Fig. 5, corresponds to $\lambda^2-\lambda^{-1}=0.61$, much less than the maximum value of $\lambda^2-\lambda^{-1}=4$ shown in Fig. 4. According to Kuhn and Grün theory Z_λ is a constant. The theory is strictly only valid as $\lambda\to1$ and Fig. 5 shows that only for $\Delta\lambda$ less than about 0.0025 (0.25% strain) Z_λ can be considered to be constant. That is, only over this small range of deformation are $\langle P_2(\cos\zeta_{\text{rep}})\rangle$ and $\lambda^2-\lambda^{-1}$ linearly related. As $\Delta\lambda$ increases beyond about 0.0025, Z_λ increases sharply to a slowly varying value, with the amount of increase depending on chain length. These slowly varying, higher values for different chain lengths occur over the ranges of values of $\Delta\lambda$ used experimentally for small deformations, say, $0.1<\Delta\lambda<0.2$, or $1.1<\lambda<1.2$, corresponding to $0.30<\lambda^2-\lambda^{-1}<0.61$ in Fig. 4. In Fig. 5, the change in Z_λ as $\Delta\lambda$ increases is larger for shorter chains, *i.e.*, the nonlinearity of the $\langle P_2(\cos\zeta_{\text{rep}})\rangle$ *versus* $\lambda^2-\lambda^{-1}$ plots in Fig. 4 is more marked for shorter chains. Overall, similar behaviour to that shown in Fig. 5 was found for PE chains [4], except that the limiting region of constant Z_λ extended to larger values of $\Delta\lambda$, reaching $\Delta\lambda=0.03$ for about 200 skeletal bonds.

Unfortunately, the limiting, constant values of Z_λ as $\Delta\lambda\to0$ in Fig. 5 are not equal to those given by Kuhn and Grün theory, for which

$$Z_\lambda = 1/5m. \tag{11}$$

The differences between the values of Z_λ predicted by Kuhn and Grün theory and those from detailed molecular modelling are shown in Fig. 6, where the values Z_λ for PET and PE chains at $\Delta\lambda=0.0025$ and 0.01, respectively, are plotted *versus* $1/m$ and compared with the values expected for Gaussian chains. It can be seen that higher values of Z_λ are predicted for freely-jointed, Gaussian chains than those given by the detailed MC modelling at values of λ very near 1. It should be noted that the limiting regions of $\lambda<1.0025$ used to evaluate Z_λ for PET in Fig. 6 are not detectable in Fig. 4 as it correspond to $\lambda^2-\lambda^{-1}=0.0075$. In this region, and in contrast to the behaviour at larger values of $\lambda^2-\lambda^{-1}$ discussed

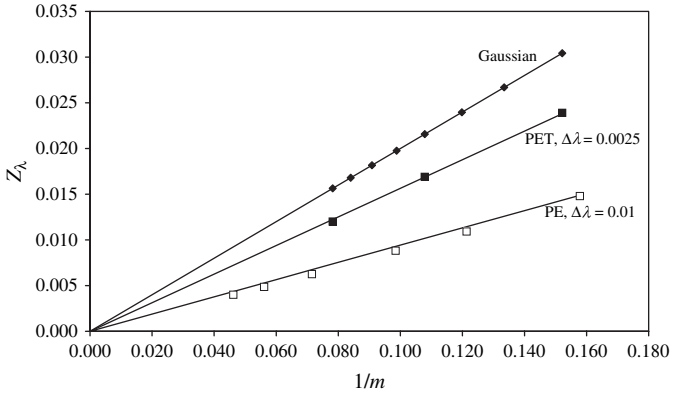

Fig. 6. Calculated limiting deformation–orientation coefficient, Z_λ, *versus* reciprocal of chain length, $1/m$, where m is the number of freely-jointed links in the statistically equivalent Gaussian chain. PET chains at 523 K. PE chains at 298 K. Gaussian points given by $Z_\lambda = 1/5m$.

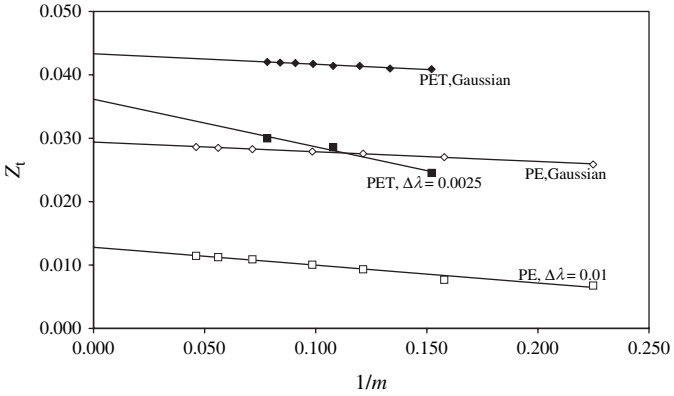

Fig. 7. Calculated limiting stress–orientation coefficient, Z_t, *versus* $1/m$. PET chains at 523 K. PE chains at 298 K. Gaussian points given by Eq. (13) or (14).

previously, the slopes of the Gaussian lines in Fig. 4 (*i.e.*, the values of Z_λ) are *higher* than those predicted by the MC modelling.

In Fig. 6, PET chains show less deviation from Gaussian behaviour than PE chains. This relative behaviour is consistent with their stress–strain behaviour, where the deviations of PET chains from affine, Gaussian behaviour were found to be less than those of PE chains [21,22]. Although the PET repeat-unit structure is relatively stiff because of the terephthaloyl unit, the *cis–trans* isomerism of that unit and the flexibility of the glycol unit mean that the repeat-unit vector easily changes its orientation over a large range of angles. Hence, the directions of sequential repeat units are only loosely correlated with each other and the chain approaches freely-jointed behaviour more closely than the PE chain, for which more than 10 skeletal bonds are equivalent to 1 freely-jointed link. As stated previously, for the PET chain, 1 repeat unit is approximately equivalent to 1 freely-jointed link.

Related to Z_λ is the stress–orientation coefficient, Z_t [3,4]

$$Z_t = \left(\frac{\langle P_2(\cos\zeta_{\text{rep}}) \rangle RT\rho}{t} \right)_{\lambda \to 1}. \tag{12}$$

From Eqs. (12) and (4) and the Gaussian stress–strain relationship (Eq. (1) with $s = 1/2$ and $\mathrm{d}s/\mathrm{d}\lambda = 0$), the Kuhn and Grün expression for Z_t can be written

$$Z_t = \frac{M_c}{5m} = \frac{M_o}{5}\frac{n}{m}. \tag{13}$$

As usual, M_c is the molar mass of the network chains of m equivalent links or n skeletal bonds and M_o is the average molar mass per skeletal bond. Comparison with Eq. (11) shows that

$$Z_t = M_c Z_\lambda. \tag{14}$$

Hence, as with Z_λ, if linear behaviour between $\langle P_2(\cos\zeta_{\text{rep}}) \rangle$ and $\lambda^2 - \lambda^{-1}$ over different ranges of $\Delta\lambda$ is assumed then different values of Z_t will result. Accordingly, if Z_t is plotted *versus* $\Delta\lambda$ then plots similar in shape to those shown in Fig. 5 for Z_λ *versus* $\Delta\lambda$ are found. As may be expected from the Kuhn and Grün expressions for Z_t, Eq. (13), the limiting values at $\lambda \approx 1$ are less sensitive to chain length than the limiting values of Z_λ shown in Fig. 6. The insensitivity occurs because the characteristic ratio n/m, the number of skeletal bonds per freely-jointed link, is only a slowly varying function of n or m. The variation of Z_t with $1/m$ is shown in Fig. 7 for PET and PE chains and for their equivalent, freely-jointed counterparts, with Z_t evaluated from Eq. (13) or (14). Again, as for Z_λ, Gaussian Kuhn and Grün theory gives values of Z_t that are too large and the differences between Kuhn and Grün chains and real chains are smaller for PET than for PE.

Eqs. (3) and (12) show that the stress–orientation coefficient, Z_t may be related to the experimental stress–optical coefficient, C, by the equation

$$Z_t = \frac{CRT\rho}{\Delta\tilde{n}_{\max}}. \tag{15}$$

Accordingly, Fig. 8 shows stress–optical plots with the experimental and calculated results of Fig. 3 for chains of 10 repeat units, together with the values of $\Delta\tilde{n}$ for infinitely long Gaussian chains, calculated using $\Delta\tilde{n}_{\max} = 0.262$, corresponding to the Denbigh bond polarisabilities. Eqs. (3), (13) and (15)

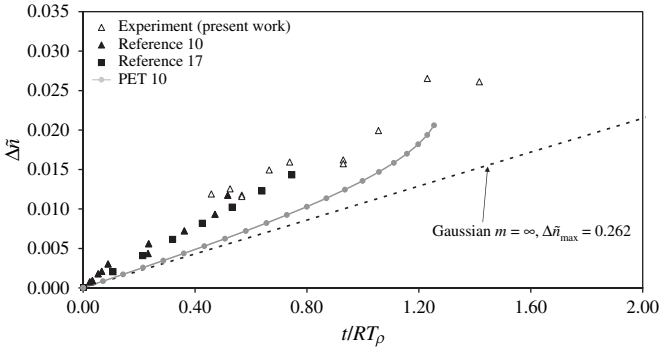

Fig. 8. Experimental and calculated birefringence–stress (stress–optical) behaviour of PET plotted as $\Delta\tilde{n}$ *versus* $t/RT\rho$. Details as Fig. 3 together with limiting plots for infinitely long Gaussian chains according to Kuhn and Grün theory, Eq. (16).

show that the dashed, Gaussian Kuhn and Grün line in Fig. 8 is described by the equations

$$\Delta\tilde{n} = Z_t \Delta\tilde{n}_{\max} \frac{t}{RT\rho} = \frac{M_o}{5}\left(\frac{n}{m}\right)_\infty \Delta\tilde{n}_{\max} \frac{t}{RT\rho}, \quad (16)$$

where $(n/m)_\infty$ is the limiting value of n/m for infinitely long chains. Considering first the theoretical and modelling results, it can be seen that Kuhn and Grün theory and the detailed MC modelling apparently agree at low stresses, *i.e.*, in other words, as $\lambda \to 1$. This agreement is not expected from Fig. 7 and it occurs because the region of very small stress or deformation ($\lambda < 1.0025$ or $\Delta\lambda < 0.0025$), where the results of the detailed MC modelling and Kuhn and Grün theory do not agree, is too small to be detected in Fig. 8. The points shown in Fig. 8 from the detailed MC modelling come from values of Z_t or Z_λ at the larger values of $\Delta\lambda$ (see Fig. 5). At these values of $\Delta\lambda$, the values of Z_t for PET from Kuhn and Grün theory shown in Fig. 7 happen to agree approximately with those from the detailed MC modelling. Thus, the agreement at small stresses shown in Fig. 8, although useful, is fortuitous. Indeed, for PE, Kuhn and Grün theory cannot be used as it gives values of the stress–optical coefficient that overestimate those from detailed MC modelling at the larger values of $\Delta\lambda$ (>0.1) by some 25% [5,6].

Comparison of the experimental with the theoretical and MC-modelling results in Fig. 8 shows that, for PET, both Kuhn and Grün theory and detailed molecular modelling using the Denbigh polarisabilities predict a stress–optical coefficient at the lower end of the experimentally attainable deformations or stresses that is about 0.67 (=1/1.5) of the measured value. (Use of the Bunn and Daubeny bond polarisabilities predicts a coefficient that is about 0.59 of the measured value and use of the LeGrand and Scacchetti bond polarisabilities predicts a coefficient that is about 0.75 of the measured value.) The agreement between Kuhn and Grün theory and the results of detailed molecular modelling in the region of experimentally accessible deformations mean that birefringence measurements can, in fact, easily be applied to calculate the residual stress in melt-spun PET. The measured value of $\Delta\tilde{n}$, together with the dashed Kuhn and Grün line of Fig. 8 for $\Delta\tilde{n}_{\max} = 0.262$ can be used to predict a value of stress; this value is then simply multiplied by about 0.67 to give the actual stress.

6. Conclusions

Using combined measurements of segmental orientation, conformational population, deformation, birefringence and stress, together with detailed molecular modelling, it has been possible to explain the deformation-related properties of bulk PET. The origin of the previously observed difference between stress–strain and stress–optical behaviour has been clarified.

The IR measurements and molecular modelling in Paper I have shown that the change of average orientation of the terephthaloyl units and the change of % *gauche* glycol conformers with deformation are consistent with bulk PET behaving as an entangled network having chains of about 10 repeat units in length (Figs. 7 and 9, Paper I). The effects of crystallisation occurring when $\lambda \approx 2.5$ are apparent in an increase in density and a faster decrease in % *gauche* glycol conformers as λ increases above this value (Figs. 6 and 7, Paper I).

Paper II established the protocols for calculating $\Delta\tilde{n}$ of PET accounting for the detailed chain structure and the conformational flexibility of the repeat unit. Accordingly, Fig. 1(a) and (b) show that, in agreement with the orientation and conformational results of Paper I, the changes in $\Delta\tilde{n}$ as a function of deformation follow the behaviour expected for chains of 9–11 repeat units. This range of chain lengths encompasses the predictions resulting from the use of the Bunn and Daubeny, Denbigh, and LeGrand and Scacchetti bond polarisabilities.

The measured stress as a function of λ is less than that expected from the measured segmental orientation, conformational population and birefringence of a network in which all the chains of 9–11 repeat units in length are assumed to be elastically active (Fig. 2). The present combined measurements of terephthaloyl orientation, % *gauche* glycol conformations, birefringence and stress show that (in contrast to earlier conclusions) it is the measured stress that is lower than expected and not the birefringence that is too high. The entanglements that define the network chains and the segment-based properties (orientation, conformations, birefringence) are not all sufficiently permanent to support stress or not all the network chains are elastically active. It should be possible to test the validity of this conclusion by studying PET networks with permanent junction points. Also, the fraction of entanglements that is elastically active could well depend on the rate at which strain is applied. This possibility also needs further investigation. Due to the low measured values of stress, the stress–optical coefficient is about 1.5 times higher than expected on the basis of the Denbigh bond polarisabilities (Fig. 3). The corresponding factors for the Bunn and Daubeny and LeGrand and Scacchetti bond polarisabilities are 1.7 and 1.3, respectively.

Comparison of the MC-modelling results with the predictions of Kuhn and Grün theory shows that the latter is quantitatively in error regarding the dependence of repeat-unit orientation on deformation (Fig. 4). Moreover, the MC modelling shows that the deformation–orientation coefficient, Z_λ, is not constant, independent of deformation (Fig. 5). Kuhn and Grün theory applies to the region $\lambda \to 1$. However, at very small deformations, the values of Z_λ and the stress–orientation coefficient, Z_t, for different chain lengths are shown to be overestimated by Kuhn and Grün theory (Figs. 6 and 7). Also, the differences between the results of Kuhn and Grün theory and those of the MC molecular modelling are found to be larger for PE chains than for PET chains. This relative behaviour is attributed to the smaller deviations of PET chains from affine Gaussian behaviour at small strains compared with those shown by PE chains. If calculated results for PET at the (larger) deformations accessible experimentally are used, Kuhn and Grün theory and detailed MC modelling are found to predict similar stress–optical coefficients (Fig. 8). Such

an agreement is fortuitous and is not found for PE chains, where Kuhn and Grün theory gives a stress–optical coefficient that is some 25% too large. The agreement in the case of PET does, however, enable measured values of $\Delta\tilde{n}$ to be used to predict, in a semi-empirical fashion, the stress in the melt-spun polymer.

As deformation or stress is increased further, comparison between the results of detailed MC modelling and Kuhn and Grün theory for PET shows that the latter increasingly underestimates Z_λ and Z_t (Figs. 4 and 8). This behaviour is different from that found previously for PE [4], for which, at shorter chain lengths, the values of Z_λ and Z_t are lower than those from the detailed MC modelling, as for PET. However, at longer chain lengths the Kuhn and Grün values of Z_λ and Z_t become higher than those from the detailed MC modelling. Thus, Kuhn and Grün predictions are, in general, difficult to use as the sense and the size of their deviations from actual molecular behaviour are dependent on chain structure.

Acknowledgement

The authors gratefully acknowledge the financial support of the EPSRC.

References

[1] Kuhn W, Grün F. Kolloid Z 1942;101:248.
[2] Treloar LRG. The physics of rubber elasticity. 3rd ed. Oxford: Clarendon Press; 1975.
[3] Taylor DJR, Stepto RFT, Jones RA, Ward IM. Macromolecules 1999;32:1978.
[4] Cail JI, Taylor DJR, Stepto RFT, Brereton MG, Jones RA, Ries ME, et al. Macromolecules 2000;33:4966.
[5] Ries ME, Brereton MG, Ward IM, Cail JI, Stepto RFT. Macromolecules 2002;35:5665.
[6] Cail JI, Stepto RFT, Ward IM. J Macromol Sci Part B Phys 2005;44:843.
[7] Saunders DW. Trans Faraday Soc 1956;52:1425.
[8] Stepto RFT, Taylor DJR. Macromol Symp 1995;93:261.
[9] Stepto RFT, Taylor DJR. J Chem Soc Faraday Trans 1995;91:2639.
[10] Pinnock PR, Ward IM. Trans Faraday Soc 1966;62:1308.
[11] Nobbs JA, Bower DI, Ward IM. J Polym Sci Polym Phys Ed 1979;17:259.
[12] Cunningham A, Willis HA, Zichy V, Ward IM. Polymer 1974;15:749.
[13] Gordon DA, Duckett RA, Ward IM. Polymer 1994;35:2554.
[14] Kashiwagi M, Cunningham A, Manuel AJ, Ward IM. Polymer 1973;14:111.
[15] Cunningham A, Manuel AJ, Ward IM. Polymer 1976;17:125.
[16] Ward IM. Proc Phys Soc 1962;80:1176.
[17] Ward IM, Bleackley M, Taylor DJR, Cail JI, Stepto RFT. Polym Eng Sci 1999;39:2335.
[18] Saunders LS, Ward IM, Cail JI, Stepto RFT. Polymer 2007;48:1360.
[19] Cail JI, Stepto RFT, Taylor DJR, Jones RA, Ward IM. Phys Chem Chem Phys 2000;2:4361.
[20] Cail JI, Stepto RFT. Polymer 2003;44:6077.
[21] Saunders LS, Ward IM, Cail JI, Stepto RFT. Polymer 2004;45:2357.
[22] Cail JI, Stepto RFT, Ward IM. Polymer 2007;48:1367.
[23] DuPont U.K. Private communication.
[24] Denbigh KG. Trans Faraday Soc 1940;36:936.
[25] Bunn CW, Daubeny R de P. Trans Faraday Soc 1954;50:1173.
[26] LeGrand DG, Scacchetti PA. Intrinsic birefringence of polymers. GE Global Research, <http://www.crd.ge.com/cooltechnologies/pdf/1999069.pdf>; 1999 [accessed 29.08.99].
[27] Matthews RG, Duckett RA, Ward IM, Jones DP. Polymer 1997;38:4795.
[28] Ball RC, Doi M, Edwards SF, Warner M. Polymer 1981;22:1010.
[29] Ward IM. Adv Polym Sci 1985;66:81.